Molecular Crystals and Liquid Crystals

Publication details, including instructions for authors and subscription information:
http://www.tandfonline.com/loi/gmcl20

Effects of Confinement and Electric Field on the Dielectric Behavior of Smectic- Phase

U. Manna [a], Jang-Kun Song [a], A. D. L. Chandani [a] & J. K. Vij [a]

[a] Department of Electronic and Electrical Engineering, Trinity College, University of Dublin, Dublin 2, Ireland

Version of record first published: 05 Oct 2009

To cite this article: U. Manna, Jang-Kun Song, A. D. L. Chandani & J. K. Vij (2009): Effects of Confinement and Electric Field on the Dielectric Behavior of Smectic-Phase, Molecular Crystals and Liquid Crystals, 512:1, 21/[1867]-31/[1877]

To link to this article: http://dx.doi.org/10.1080/15421400903048677

Mol. Cryst. Liq. Cryst., Vol. 512, pp. 21/[1867]–31/[1877], 2009

ISSN: 1542-1406 print/1563-5287 online
DOI: 10.1080/15421400903048677

Effects of Confinement and Electric Field on the Dielectric Behavior of Smectic-C^*_α Phase

U. Manna, Jang-Kun Song, A. D. L. Chandani, and J. K. Vij
Department of Electronic and Electrical Engineering, Trinity College, University of Dublin, Dublin 2, Ireland

Dielectric permittivity measurements are carried out to investigate the effects of confinement and electric field on a chiral smectic liquid crystal in the smectic-C^*_α (Sm-C^*_α) phase for various cell thicknesses. The Sm-A^* – Sm-C^*_α transition temperature and the temperature range for which the Sm-C^*_α phase is stable decrease with decreasing cell thickness. On reducing the cell thickness, the surface-induced mode appears, as a result of the influence of the cell substrates. This increases the dielectric strength of the Sm-C^*_α phase. The distribution parameter of the relaxation process, α decreases significantly, and in the case of a thin cell, the decrease observed reflects a wide symmetric distribution of the relaxation process. On increasing the electric field, the dielectric strength decreases and the relaxation frequency increases in the Sm-C^*_α phase. These are explained by the 'helical fracture' model, originally proposed for the Sm-C^* phase.

Keywords: confinement effects; dielectric spectroscopy; Sm-C^*_α phase; transition temperature

I. INTRODUCTION

Several theoretical approaches have been considered over the years to explain a variety of liquid crystalline phases based on the Landau model [1,2], Ising model [3] and clock model [4,5]. The short pitch helical structure of the frustrated Sm-C^*_α phase was obtained by minimizing the free energy of the system containing competing interactions between the nearest and the next nearest smectic layers [4], and the fact that the tilt angle varies with temperature was used to understand the dielectric and dynamical properties of the phase [6,7]. The Sm-C^*_α phase has been extensively studied by various experimental

Address correspondence to J. K. Vij, Department of Electronic and Electrical Engineering, Trinity College, University of Dublin, Dublin 2, Ireland. E-mail: jvij@tcd.ie

techniques such as differential scanning calorimetry, x-ray diffraction, electro-optic response, dielectric response and Raman scattering [8–11]. The short pitch helical structure of the Sm-C^*_α phase was experimentally confirmed through resonant x-ray scattering experiments [12,13]. The switching behavior of the Sm-C^*_α phase was also explained by considering the antiferroelectric aspect of the helical structure recently [14]. Dielectric observations show that the Sm-A^* – Sm-C^*_α transition is revealed by a change in the slope of the temperature dependence of the dielectric strength of the soft mode [15,16]. The compound 12OF1M7 has extensively been studied under the name AS-573 to investigate the ferrielectric subphases with high q_T parameter [17], the relaxation processes in antiferroelectric liquid crystalline phases [18], and the field-induced phase transitions [19]. The series of nF1M7 chiral liquid crystalline compounds, where n denotes the length of the unbranched terminal chain, were studied by dielectric spectroscopy for different cell thicknesses showing that the dielectric response is dominated by the surface induced structures if the cell gap is reduced and reflecting that the bulk thermodynamic phase exists in a very thick cell [20]. The optical reflectivity measurement on 12OF1M7(R) was also performed to confirm the existence of the Sm-C^*_α phase with nano-scale helical pitch [21]. The influence of dc bias on the Sm-C^*_α phase was also investigated to confirm the helical structure of the phase, which is strongly modified under dc bias field [16,22].

We carry out the dielectric spectroscopy measurement to investigate the effects of confinement and electric field in the Sm-C^*_α phase for various cell thicknesses under the influence of electric field in 12OF1M7(R). The stability of the Sm-C^*_α phase is investigated by finding the transition temperatures for the various cell thicknesses. We find that on reducing the cell thickness, the surface-induced mode along with the soft mode results in an increase of the dielectric strength in the Sm-C^*_α phase. We also find that on increasing the electric field, the dielectric strength decreases and relaxation frequency increases in the Sm-C^*_α phase. This has been explained by the 'helical fracture' model, originally proposed for Sm-C^*_α phase [23].

II. EXPERIMENTAL

The Anti-Ferroelectric Liquid Crystal (AFLC) sample, 12OF1M7(R) synthesized by Kingston Chemical, Hull, U.K., with the structure as shown in Figure 1, was investigated for cell thicknesses varying from 3 to 80 μm. The thickness of the liquid crystal cell was measured based on the measurements of the transmittance spectra of a UV-visible

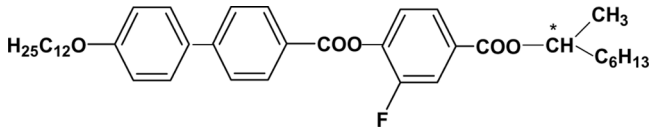

FIGURE 1 Chemical structure of 12OF1M7(R).

spectrometer (AvaSpec-2048) using the interference fringes caused by the reflection from two parallel glass surfaces of the cell closely separated from each other. The cell thickness was calculated using the following formula:

$$d = \frac{\lambda_k \lambda_{k+n} n}{2(\lambda_{k+n} - \lambda_k)} \tag{1}$$

where λ_k and λ_{k+n} are the wavelengths of two maxima (minima) seperated by n minima (maxima) correspondingly. The electric-field-induced birefringence of 12OF1M7(R) was measured for a 25 μm thick homeotropic cell by applying an in-plane electric field. The gap between the electrodes was 180 μm. The details of the measurement are given in reference [24]. We measured the field-induced birefringence at each temperature by changing the applied field in 100 steps. The temperature was lowered at a rate of 0.01°C/min. To assure thermal equilibrium, the sample was kept at each measuring temperature for 1 min before starting to change the field. The dielectric measurements were performed on cooling the sample from 110°C to 60°C. Sample cells for low frequency (<1 MHz) dielectric measurements consisted of a planar capacitor made of two chemically etched ITO coated glass plates with sheet resistance 20 Ω/□. For planar alignment, the conducting inner surfaces were spin coated with a polyimide RN 1175 (Nissan Chemicals) alignment layer and rubbed parallel.

III. RESULTS AND DISCUSSIONS

The Sm-C^*_α phase was identified by electric field induced birefringence and dielectric spectroscopy measurement in 12OF1M7(R). Figure 2 shows the electric-field-induced birefringence measured in the cooling cycle in 25 μm homeotropic cells of nominally pure 12OF1M7(R) to confirm the existence of Sm-C^*_α phase in the cooling process. The field-induced birefringence apparently increases during the unwinding process in the chiral smectic phases. Much more evidently, each phase shows its characteristic pattern of the birefringence contours. When the applied electric field is sufficiently high, all the phases

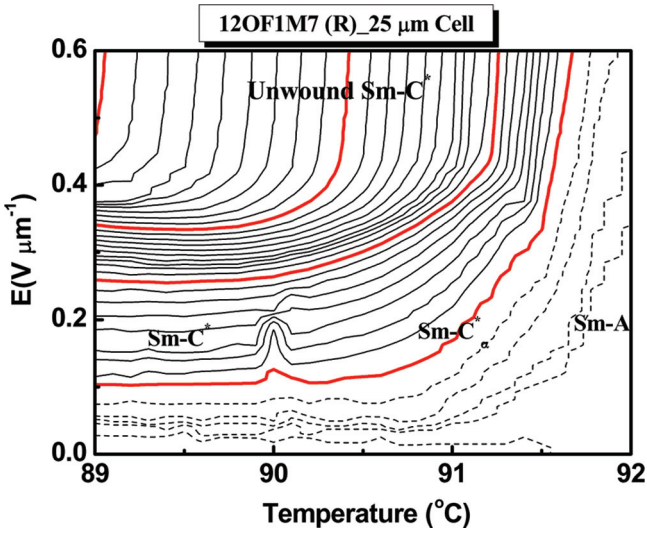

FIGURE 2 Electric-field-induced birefringence measured in the cooling cycle in 25 μm homeotropic cells of nominally pure 12OF1M7(R). This shows the existence of Sm-C^*_α phase in the cooling process. The birefringence contours drawn in solid lines are at steps of 0.5×10^{-4} and some auxiliary lines in smaller steps are drawn in dotted lines.

under consideration become unwound Sm-C^*. The birefringence contours in principle is then parallel to the electric field, E-axis, as obviously seen in the figure. The electroclinic effect plays an important role in the Sm-A^* phase and the birefringence contours linearly rise with an increase in the applied electric field as seen in the above figure. In the Sm-C^* phase the helix starts to unwind even rather at low fields resulting in a large birefringence, contour lines are horizontal and parallel to the temperature axis at lower field and becomes vertical at higher field when the helix is completely unwound. In contrast, the unwinding process of the ultra short-helical pitch in Sm-C^*_α requires relatively higher field than that required in ordinary Sm-C^* phase. The phase transition from Sm-C^*_α into unwound Sm-C^* requires relatively high field but becomes lower with falling temperature as the short pitch becomes longer. In the temperature region just below Sm-A^*, the birefringence contour lines curved up finally becoming vertical in the complete unwound state. According to the E-T phase diagram there exists Sm-C^*_α below Sm-A^* phase in a very narrow temperature range of about 1.2°C. However, the transition from Sm-C^*_α to Sm-C^* apparently occurs continuously indicating a second order phase

transition. The photoelastic modulator-based set up was used to measure the electric field induced birefringence of the various subphases of 12OF1M7 [25].

The dielectric response was studied for eight different cell thicknesses ranging from 3 to 80 μm to find the dependence of phase transition temperatures (T_c), dielectric strength ($\Delta\varepsilon$) and relaxation frequency (f_{max}) on the cell thickness in the Sm-C^*_α phase. Experimental observations showed that the Sm-A^* – Sm-C^*_α phase transition is only noticed by a change in the slope of the temperature dependence of the dielectric strength of the soft mode [15,16]. The first change in the slope is due to an increase in the amplitude of soft mode close to the Sm-A^* – Sm-C^*_α transition and the second is due to a decrease and then increase in the strength of Goldstone mode at the Sm-C^*_α – Sm-C^* transition. The transition temperatures for the Sm-C^*_α phase are determined by plotting the temperature dependence of the real part of the permittivity (ε') for different frequencies as shown in Figure 3 for (a) 50, (b) 25 and (c) 10 μm cell thicknesses. The transition temperatures are determined from the ε' dependence on temperature at 22 kHz for all the cells.

Figure 4 shows the cell thickness dependence of the temperature range for which Sm-C^*_α phase is stable. We find that the temperature range of the Sm-C^*_α phase decreases slowly with decreasing thickness up to a critical thickness of about 9 μm. After that, the temperature range decreases very rapidly. This behavior can be explained by considering the contribution of the free energy induced by the unit surface [26].

Figure 5 shows dependence of dielectric strength ($\Delta\varepsilon$), relaxation frequency (f_{max}) and distribution parameter (α) on temperature in the Sm-C^*_α phase for thicknesses of 50, 25, and 10 μm. These are found by fitting the imaginary part of dielectric permittivity (ε'') to the Havriliak-Negami equation. The Havriliak-Negami equation for n relaxation processes is given by [27]

$$\varepsilon^*(\omega) = \epsilon' - i\varepsilon'' = \varepsilon_\infty + \sum_{i=1}^{n} \frac{\Delta\epsilon_i}{[1 + (j\omega\tau_i)^{\alpha_i}]^{\beta_i}} - \frac{i\sigma_{dc}}{\varepsilon_0\omega} \tag{2}$$

where ε_∞ is the high-frequency permittivity, i is a variable denoting the number of relaxation processes up to n, τ_i and $\Delta\varepsilon_i$ are the relaxation time and the dielectric strength of the ith process, α_i and β_i are the corresponding fitting parameters. The term $(-j\sigma_{dc}/\varepsilon_0\omega)$ takes account of the dielectric loss due to the ionic conduction. Ionic conduction contributes to the dielectric spectra at low frequencies. σ_{dc} is the dc conductivity, ω and ε_0 are the angular frequency and the permittivity of the

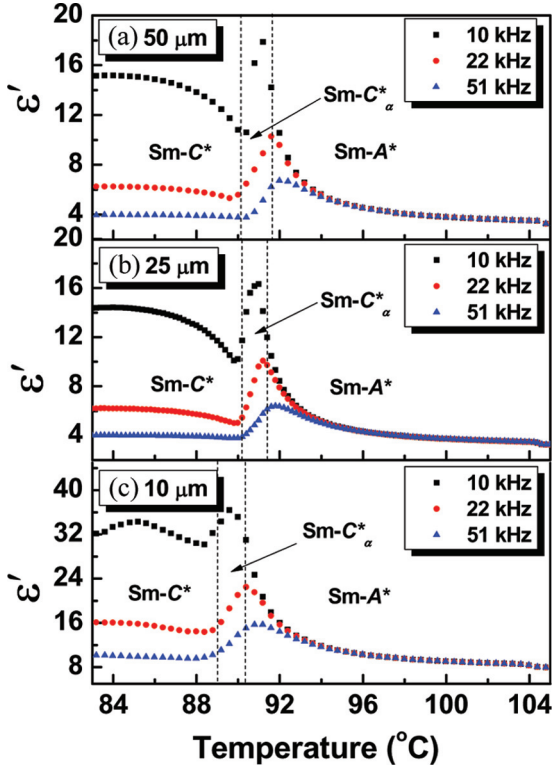

FIGURE 3 Dependence of real part of the dielectric permittivity (ε') on temperature for the different frequencies in 12OF1M7(R) for cell thickness of 50 (a), 25 (b) and 10 μm (c).

free space, respectively. The Sm-C^*_α phase normally shows a contribution to $\Delta\varepsilon$ due to azimuthal angle fluctuations, which indicates that in the Sm-C^*_α phase, we no longer see a pure soft mode, but a mixture of soft and Goldstone modes. On reducing the cell gap, we see the appearance of a mode that is not inherent of the phase but is a result of the influence of the cell substrates. Obviously, such a mode will get stronger the thinner the cell gap, as then the influence of the substrates dominates the response of the whole sample. This is why we get increasing $\Delta\varepsilon$ on reducing the cell thickness. We also see that below the phase transition temperature the distribution parameter α decreases in magnitude and the decrease is quite large for 10 μm cell. The decrease in distribution parameter on reducing the cell thickness shows that the mode is no longer a pure Debye relaxation mode. The

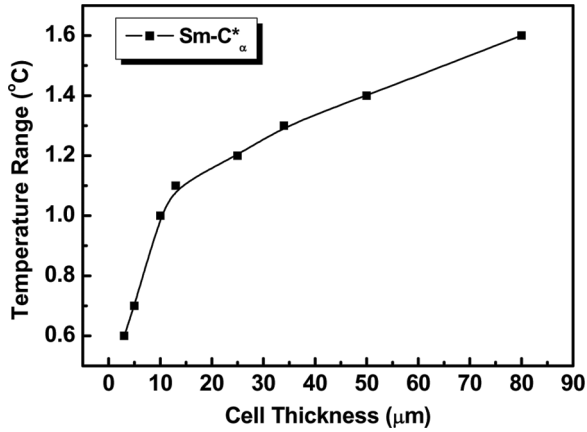

FIGURE 4 Cell thickness dependent temperature range for which the Sm-C^*_α phase is stable in 12OF1M7(R).

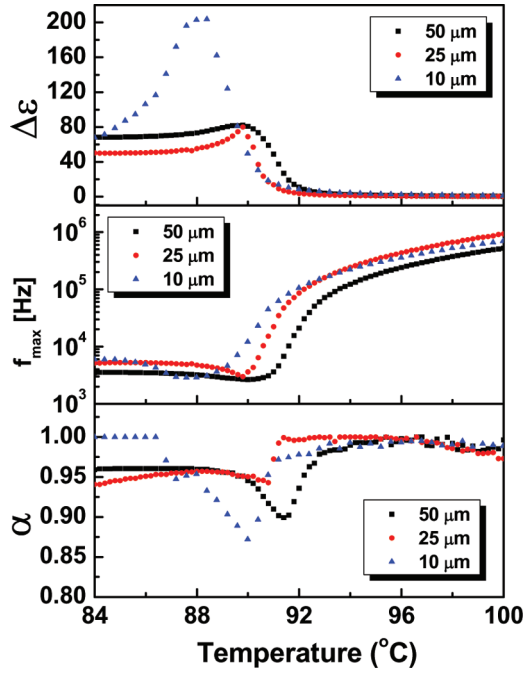

FIGURE 5 Dependence of dielectric strength ($\Delta\varepsilon$), relaxation frequency (f_{max}) and distribution parameter (α) on temperature in the Sm-C^*_α phase of 12OF1M7(R) for thickness of 50, 25, and 10 μm.

most likely reason is that the response no longer reflects a single mode, but indeed two modes. One of them is of course the soft mode but the other may be a surface-induced mode and this grows in importance as the cell thickness is decreased.

Figure 6 shows the dependence of dielectric strength ($\Delta\varepsilon$), relaxation frequency (f_{max}) on dc bias in the Sm-C^*_α phase for various thicknesses of 50, 25, and 10 μm. The $\Delta\varepsilon$ and f_{max} in the Sm-C^*_α phase are strongly modified under bias and it is probably connected with the ferroelectric like structure of this phase. The behavior of $\Delta\varepsilon$ and f_{max} under the influence of electric field in the Sm-C^*_α phase can be explained by an unwinding model based on helical fractures originally proposed for Sm-C^* phase [23,28]. In this model, the applied field increases the stress on the helix, and the stress is released by the helix getting fractured followed by the propagation of domain wall. Here, the helical pitch increases with the helical fractures, because each π

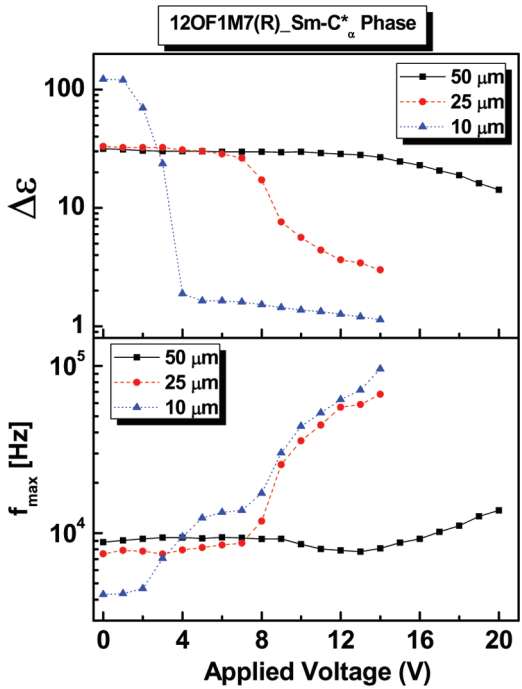

FIGURE 6 Dependence of dielectric strength ($\Delta\varepsilon$), relaxation frequency (f_{max}) on dc bias in the Sm-C^*_α phase of 12OF1M7(R) for various thickness of 50, 25, and 10 μm.

wall propagation reduces the helix by about half a turn. This is fundamentally different from a continuous increase in the helical pitch expected from the diverging pitch model [29]. The expression for electric field dependent $\Delta\varepsilon$ and f_{max} based on the non-diverging pitch model, can be calculated from the well-known free-energy expression and the corresponding Euler-Lagrange equation from the dependence of the azimuthal angle as a function of the distance along the layer normal $\phi(z) = qz + \Sigma\phi_i \sin[(i+1)qz]$, where $i = 0, 1, \ldots\ldots$, as follows:

For low fields;

$$\Delta\varepsilon_{G,l} \simeq \frac{P_s A}{32\varepsilon_0}\left[16 + \frac{2P_s^2 E_{dc}^2}{K^2 q^4} - 9\frac{P_s^4 E_{dc}^4}{K^4 q^8}\right] \tag{3}$$

$$f_{G,l} = \frac{Kq^2}{2\pi\gamma} \tag{4}$$

where $\Delta\varepsilon_{G,l}$ and $f_{G,l}$ are the dielectric strength and the relaxation frequency of the Goldstone mode at low fields. q ($=2\pi/p$, where p is pitch) is the wave vector, P_s is the spontaneous polarization, K is the elastic constant and γ is rotational viscocity. As shown in Eqs. (3) and (4), the relaxation frequency of the Goldstone mode does not depend on the dc bias at low fields, while the dielectric strength decreases slightly with the dc bias.

And for higher fields;

$$\begin{aligned}\langle P_E\rangle_h &= \frac{2z_0 P_s}{p} + \frac{(p-2z_0)P_s}{p}\left[\frac{7}{16} + \frac{5}{16}\delta\phi_0 e^{jwt}\right] \\ &= \frac{P_s}{16\rho}[16\rho - 9q + 5q\delta\phi_0 e^{jwt}]\end{aligned} \tag{5}$$

$$\Delta\varepsilon_{G,h} = \frac{5qP_s}{16\varepsilon_0\rho E_{dc}} = \sqrt{\frac{5q^2 K P_s}{64\varepsilon_0^2 E_{dc}^3}} \tag{6}$$

$$f_{G,h} = \frac{K\rho^2}{2\pi\gamma} = \frac{5P_s E_{dc}}{8\pi\gamma} \tag{7}$$

Here, $\rho = 2\pi/(p - 2z_0)$ is the effective wave vector. $\Delta\varepsilon_{G,h}$ and $f_{G,h}$ are the dielectric strength and the relaxation frequency of the Goldstone mode at higher fields. P_E is the component of P_s parallel to the applied field, and $P_E = P_s \cos\phi$. As shown in Eqs. (6) and (7), both the dielectric strength and the relaxation frequency are found to depend strongly on the amplitude of the dc bias at large fields. The dielectric strength decreases and the relaxation frequency increases with increasing field,

which is in agreement with the experimental results shown in Figure 6. However, the mechanism does not arise from the nonlinearity of K, but from an increase in the effective wave vector ρ. That is, the high bias field increases z_0 and reduces the effective pitch $(p - 2z_0)$, which in turn increases the relaxation frequency.

IV. CONCLUSION

The existence of Sm-C^*_α phase in 12OF1M7(R) is confirmed by dielectric spectroscopy and the electric-field-induced birefringence measurements. The dielectric strength $(\Delta\varepsilon)$, the relaxation frequency (f_{max}) and the distribution parameter (α) of Sm-C^*_α phases are very much dependent on the cell thickness. The Sm-A^* – Sm-C^*_α transition temperature and the temperature range for which the Sm-C^*_α phase is stable decreases by decreasing the cell thickness. On reducing the cell gap, the surface-induced mode that is not inherent of the phase appears and this is a result of the influence of the cell substrates. This along with the soft mode results in increasing dielectric strength and decreasing relaxation frequency in the Sm-C^*_α phase. The distribution parameter (α) decreases very much, and in the case of a thin cell, the decrease is quite large in the Sm-C^*_α phase indicating the behavior is a mixture of that of the soft mode and surface-induced modes. $\Delta\varepsilon$ decreases and f_{max} increases in the Sm-C^*_α phase under the influence of dc bias, which is not connected to the nonlinearity of K, but is related to an increase in the effective wave vector ρ with field.

REFERENCES

[1] Orihara, H. & Ishibashi, I. (1990). *Jpn. J. Appl. Phys.*, *29*, L115.
[2] Zeks, B. & Cepic, M. (1993). *Liq. Cryst.*, *14*, 445.
[3] Fukuda, A., Takanishi, Y., Isozaki, T., Ishikawa, K., & Takezoe, H. (1994). *J. Mater. Chem.*, *4*, 997.
[4] Cepic, M. & Zeks, B. (1995). *Mol. Cryst. Liq. Cryst.*, *263*, 61.
[5] Roy, A. & Madhusudana, N. V. (1996). *Europhys. Lett.*, *36*, 221.
[6] Cepic, M., Heppke, G., Hollidt, J.-M., Lotzsch, D., Moro, D., & Zeks, B. (1995). *Mol. Cryst. Liq. Cryst.*, *263*, 207.
[7] Cepic, M. & Zeks, B. (1996). *Liq. Cryst.*, *20*, 29.
[8] Fukui, M., Orihara, H., Yamada, Y. Y., Yamamoto, N., & Ishibashi, Y. (1989). *Jpn. J. Appl. Phys.*, *28*, L849.
[9] Glogarova, M., Sverenyak, H., Nguyen, H. T., & Destrade, C. (1993). *Ferroelectrics*, *147*, 43.
[10] Hiraoka, K., Taguchi, A., Ouchi, Y., Takezoe, H., & Fukuda, A. (1990). *Jpn. J. Appl. Phys.*, *29*, L103.
[11] Farhi, R., Nguyen, H. T., & Lorman, V. L. (1997). *Europhys. Lett.*, *40*, 49.
[12] Mach, P., Pindak, R., Levelut, A. M., Barois, P., Nguyen, H. T., Huang, C. C., & Furenlid, L. (1998). *Phys. Rev. Lett.*, *81*, 1015.

[13] Mach, P., Pindak, R., Levelut, A. M., Barois, P., Nguyen, H. T., Baltes, H., Hird, M., Toyne, K., Seed, A., Goodby, J. W., Huang, C. C., & Furenlid, L. (1999). *Phys. Rev. E*, *60*, 6793.
[14] Lagerwall, J. P. F. (2005). *Phys. Rev. E*, *71*, 051703.
[15] Shtykov, N. M., Vij, J. K., Panov, V. P., Lewis, R. A., Hird, M., & Goodby, J. W. (1999). *J. Mater. Chem.*, *9*, 1383.
[16] Douli, R., Legrand, C., Faye, V., & Naguyen, H. T. (1999). *Mol. Cryst. Liq. Cryst.*, *328*, 209.
[17] Panarin, Yu. P., Kalinovskaya, O., Vij, J. K., & Goodby, J. W. (1997). *Phys. Rev. E*, *55*, 4345.
[18] Panarin, Yu. P., Kalinovskaya, O., & Vij, J. K. (1998). *Liq. Cryst.*, *25*, 241.
[19] Shtykov, N. M., Vij, J. K., Lewis, R. A., Hird, M., & Goodby, J. W. (2000). *Phys. Rev. E*, *62*, 2279.
[20] Lagerwall, J. P. F., Parghi, D. D., Kruerke, D., Gouda, F., & Jagemalm, P. (2002). *Liq. Cryst.*, *29*, 163.
[21] Panov, V. P., McCoy, B. K., Liu, Z. Q., Vij, J. K., Goodby, J. W., & Huang, C. C. (2006). *Phys. Rev. E*, *74*, 011701.
[22] Rutkowska, J., Perkowski, P., Kedzierski, J., Raszewski, Z., & Kolsowicz, S. (2004). *Mol. Cryst. Liq. Cryst. 409*, 389.
[23] Song, J. K., Manna, U., & Vij, J. K. (2008). *Europhys Lett.*, *82*, 26003.
[24] Chandani, A. D. L., Shtykov, N. M., Panov, V. P., Emelyanenko, A. V., Fukuda, A., & Vij, J. K. (2005). *Phys. Rev. E*, *72*, 041705.
[25] Manjuladevi, V. & Vij, J. K. (2007). *Liq. Cryst.*, *34*, 963.
[26] Manna, U., Song, J. K., Power, G., & Vij, J. K. (2008). *Phys. Rev. E*, *78*, 021711.
[27] Havriliak, S. J. & Negami, S. (1967). *Polym.*, *8*, 161.
[28] Song, J. K., Vij, J. K., & Kobayashi, I. (2007). *Phys. Rev. E*, *75*, 051705.
[29] Meyer, R. B. (1977). *Mol. Cryst. Liq. Cryst. 40*, 33.